Geophys. J. Int. (2002) **149,** 149–156

The effects of stress and fluid pressure on the anisotropy of interconnected cracks

S. R. Tod

Department of Applied Mathematics and Theoretical Physics, University of Cambridge, Silver Street, Cambridge CB3 9EW, *UK.*
E-mail: S.R.Tod@damtp.cam.ac.uk
British Geological Survey, West Mains Road, Edinburgh EH9 3LA, *UK*

Accepted 2001 October 12. Received 2001 October 11; in original form 2001 March 21

SUMMARY

The cracks in a porous matrix that is subjected to a change in the applied stress or fluid pressure will undergo a distortion related to their orientation relative to the principal directions of the applied stress. Both the crack distribution and the fluid-flow properties of the aggregate will be altered as a consequence, of a change in either the applied stress or fluid pressure, resulting in a change in the effective elastic parameters of the material. An effective medium theory, based on the method of smoothing and incorporating a transfer of fluid between connected cracks via non-compliant pores, is used to derive an expression for the effective elastic parameters of the material, to first order in the crack density ϵ. This expression involves a dependence on both the applied stress and the fluid pressure, and is used to determine the effects on the anisotropy of the effective medium of the applied stress and the fluid pressure. A number of azimuthally symmetric compressive stresses are applied to an isotropic crack distribution to determine the material properties of the resulting transversely isotropic effective medium, as a function of the excess in compressive stress over fluid pressure. As a result of competing processes, the theory predicts that, for a non-hydrostatic stress, there is a pressure at which the anisotropy reaches a maximum value before the properties of the effective medium decay, under increasing stress, to those of the uncracked matrix. The theory does not, however, account for the material failure that will occur at large compressive stresses. Finally, the theory predicts that *S* waves are more sensitive to changes in the applied stress or fluid pressure than *P* waves.

Key words: anisotropy, cracked media.

1 INTRODUCTION

The cracks in a matrix rock are, potentially, a result of a number of competing processes (Menéndez *et al.* 1999) that dictate the resulting crack distribution. Within unstressed rock cracks exist as a result of either the mineralogy of the rock, thermal processes or stress history (e.g. Fredrich & Wong 1986). The crack orientation distribution may be anisotropic, as a result of anisotropic paleostresses. A non-isotropic stress applied to the rock will result in preferential crack closure. The greater the alignment between the crack normal and the principal directions of the stress, the less the stress needed to close any given crack. The resulting crack distribution will exhibit further anisotropy. Furthermore, an applied stress will, in general, result in the formation of new cracks (e.g. Montoto *et al.* 1995) that are likewise predominantly oriented parallel to the direction of maximum principal stress (Menéndez *et al.* 1999).

The presence of pores or cracks in matrix rock will influence the mechanical properties of the rock (Walsh 1965a,b). Thus, by modelling the crack distribution to account for the effects of stress (Nur 1971; Sayers 1988b; Gibson & Toksöz 1990) we may study the effects of the cracks on these mechanical properties, such as the velocities (Nur 1971; Kuster & Toksöz 1974; Sayers 1988b) or the permeability (Gibson & Toksöz 1990). One may then attempt to invert measurements of such properties for crack or pore parameters (Cheng & Toksöz 1979; Sayers 1988a; Sun & Goldberg 1997). Clearly, then, advancements in the modelling of the mechanical properties resulting from a distribution of cracks will aid the accuracy of inversion techniques.

The effects of the application of an ambient stress to a cracked medium has been studied both analytically (Horii & Nemat-Nasser 1983; Carlson & Gangi 1985; Li & Nordlund 1993; Pecorari 1997; Zatsepin & Crampin 1997) and experimentally (Winkler 1985; Freund 1992; Hornby 1994; Wulff *et al.* 1999) concluding that wave speeds increase with differential pressure, defined as the difference between the compressive stress and fluid pressure, whatever the form of the compression that the rock is subjected to. The behaviour of fractures under compression has also been the subject of analytic (Bai *et al.* 2000) and experimental (Brown & Scholz 1986) studies. Results are explained in terms of preferentially oriented crack

closure. However, none of these models have an explicit dependence on the flow of fluid between cracks.

The method of smoothing (Hudson 1980) i.e. an effective medium theory, gives the effective elastic parameters of a cracked material, which allows the calculation of the speeds of waves of long wavelengths. The method has recently been extended to allow for the cracks to be connected through the porosity of the matrix rock (Hudson *et al.* 1996; Tod 2001) where fluid may flow between cracks that have been distorted differently by an incident wave owing to differences in their orientation and aspect ratio. This model, up to Tod (2001), fails to account for the dependence of the crack distribution on both the applied stress field and the fluid pressure, and the fact that the distributions of crack aspect ratio and orientation are interdependent.

In this paper a model for the number density of cracks is developed that depends on both the aspect ratio and orientation of the cracks, and, furthermore, depends on both the applied stress and the fluid pressure. While Sun & Goldberg (1997) categorize the dynamic process of rock deformation under a changing differential pressure into four stages, only the first and third of these are considered in the model herein; collapse of, and closure of, the original cracks. The remaining two stages are defined as the deformation of pores into cracks and the formation of new cracks of small aspect ratio. The model developed here thus predicts that the crack density decays monotonically with an increase in the applied stress from some initial value corresponding to the unstressed state. Thus, this model is purely elastic, and assumes that during subsequent unloading, the material relaxes to its original state. The model does not therefore incorporate hysteresis (Li & Nordlund 1993; Gangi & Carlson 1996), a result of crack growth (Gangi & Carlson 1996) or crack formation (Sun & Goldberg 1997).

This model for the crack number density is used in conjunction with the dependence of the effective elastic parameters on the crack distribution, as derived by Tod (2001), to model the relation between the anisotropy of the effective medium, incorporating fluid flow, and the applied stress and fluid pressure.

2 A FLUID-FLOW MODEL

We follow the model of connected cracks proposed by Hudson *et al.* (1996) and extended by Tod (2001) for the transfer of fluid between cracks by non-compliant pores. The model is based on a local flow governed by the mass transport equation

$$\frac{\partial}{\partial t}\left(\rho_{\mathrm{f}}^{n}\phi_{n}\right) = -\frac{\phi_{n}^{0}\rho_{0}}{\kappa_{\mathrm{f}}\tau}\left(p_{\mathrm{f}}^{n} - p_{\mathrm{f}}\right), \tag{1}$$

which introduces attenuation into the model, and a global flow resulting from D'Arcy's law and the conservation of mass,

$$\frac{\partial}{\partial t}\left(\sum_{n}\rho_{\mathrm{f}}^{n}\phi_{n}\right) = \nabla\cdot\left(\frac{\rho_{\mathrm{f}}}{\eta_{\mathrm{f}}}\boldsymbol{K}^{r}\cdot\nabla p_{\mathrm{f}}\right), \tag{2}$$

where ϕ_n, ϕ_n^0, ρ_{f}^n and p_{f}^n are the porosity, stress-free porosity, fluid density and fluid pressure, respectively, in the nth set of cracks, where the cracks have been divided into families of parallel cracks with identical aspect ratio and radius. ρ_0 is the unstressed density, κ_{f} the bulk modulus of the fluid, ρ_{f} the average fluid density, p_{f} the average (local) pressure in the fluid, η_{f} the fluid viscosity, $\boldsymbol{K}^r$ the permeability tensor of the matrix and τ a relaxation parameter that characterizes the timescale of pressure equalization between neighbouring cracks. The model is only valid at low pore porosities. A basis for eq. (1) is given in Appendix A of Tod (2001), where it is erroneously referred to as a diffusion equation.

This model is used by Tod (2001) to derive an expression, in frequency–wavenumber space, for the effective elastic parameters of a cracked material to first order in the crack density ϵ;

$$\boldsymbol{c} = \boldsymbol{c}^{0} + \epsilon\boldsymbol{c}^{1} + \mathcal{O}(\epsilon^{2}), \tag{3}$$

where $\boldsymbol{c}^0$ is the elastic tensor for the, assumed isotropic, porous matrix material,

$$c_{ipjq}^{0} = \lambda\delta_{ip}\delta_{jq} + \mu(\delta_{ij}\delta_{pq} + \delta_{iq}\delta_{jp}), \tag{4}$$

with λ and μ being the Lamé constants of the material; $\boldsymbol{c}^1$ accounts for scattering off individual cracks.

3 THE EFFECTS OF STRESS AND FLUID PRESSURE ON THE ASPECT RATIO

A change in the stress and/or fluid pressure on a cracked material will result in a distortion of the cracks, which will alter the effective elastic parameters. Hudson (2000) derives an expression for the change in crack aspect ratio $\delta\alpha$ caused by a change in applied stress field $\delta\boldsymbol{\sigma}$ and fluid pressure δp_{f} on a crack, the normal of which lies in the direction $\mathbf{n}$;

$$\delta\alpha = \frac{2(1-\nu)}{\pi\mu}(\delta\sigma_{ij}n_{i}n_{j} + \delta p_{\mathrm{f}}) - \frac{\alpha}{\kappa}\delta p_{\mathrm{f}}, \tag{5}$$

where ν is Poisson's ratio for the matrix material. The last term on the right-hand side is neglected by Hudson (2000) in comparison with the other terms. This result is also given by Walsh (1965a) and Zatsepin & Crampin (1997), without the last term. The sign convention is such that a positive $\delta\boldsymbol{\sigma}$ or δp_{f} will cause the cracks to open. Integrating eq. (5), we find that

$$\ln\left(\frac{1+k_{r}\alpha}{1+k_{r}\alpha_{0}}\right) = \frac{2k_{r}(1-\nu)}{\pi\mu}(\sigma_{ij}n_{i}n_{j} + p_{\mathrm{f}}), \tag{6}$$

where α_0 is the aspect ratio of a given crack in the absence of stress and fluid pressure and

$$k_{r} = -\frac{3\pi(1-2\nu)}{4(1-\nu^{2})} \tag{7}$$

is an $\mathcal{O}(1)$ constant. Expanding the left-hand side of eq. (6) as a Taylor series yields

$$\alpha - \frac{k_{r}}{2}\left(\alpha^{2} - \alpha_{0}^{2}\right) + \mathcal{O}\left(\alpha^{3} - \alpha_{0}^{3}\right) = \alpha_{0} + \frac{2(1-\nu)}{\pi\mu}(\sigma_{ij}n_{i}n_{j} + p_{\mathrm{f}}), \tag{8}$$

and for small aspect ratios we may neglect all terms of $\mathcal{O}(\alpha^2 - \alpha_0^2)$ or above, such that

$$\alpha = \alpha_{0} + \frac{2(1-\nu)}{\pi\mu}(\sigma_{ij}n_{i}n_{j} + p_{\mathrm{f}}). \tag{9}$$

Attention is restricted to three alternative forms of compression: uniaxial, biaxial and hydrostatic. For the uniaxial and biaxial forms, the axis of symmetry is taken to be the x_3-axis. This is the axis of maximum stress for uniaxial compression and the axis of minimum stress for biaxial compression. The corresponding stress tensors are given by

$$\sigma_{ij}^{\mathrm{U}} = -\sigma\delta_{i3}\delta_{j3}, \tag{10}$$

$$\sigma_{ij}^{\mathrm{B}} = -\sigma(\delta_{i1}\delta_{j1} + \delta_{i2}\delta_{j2}), \tag{11}$$

and

$$\sigma_{ij}^{\mathrm{H}} = -\sigma\delta_{ij}, \tag{12}$$

respectively. We then have that the differential pressure is given by

$$p_{\mathrm{d}} \equiv -\left(\max_{1\le i\le 3}\{-\zeta^i\} + p_{\mathrm{f}}\right) = \sigma - p_{\mathrm{f}}, \tag{13}$$

where the ζ^i correspond to the eigenvalues of the tensile stress tensor $\{\sigma_{ij}\}$. The differential pressure is a measure of the closing pressure on the cracks, where the compressive stress works to close the cracks, to which the fluid pressure provides a resistance.

On the application of a uniaxial compression (eq. 10) in the absence of fluid pressure, eq. (9) yields a critical angle, θ_0, for the crack normal below which a crack with initial aspect ratio α is closed:

$$\cos^2\theta_0 = \frac{\pi\mu\alpha}{2(1-\nu)\sigma}. \tag{14}$$

This result differs from that given by Gibson & Toksöz (1990) as a result of an approximation made by Walsh (1965a). The corresponding result for biaxial compression is

$$\sin^2\theta_0 = \frac{\pi\mu\alpha}{2(1-\nu)\sigma}. \tag{15}$$

4 EFFECTIVE ELASTIC PARAMETERS

The expression derived for the first-order correction to the effective elastic parameters by Tod (2001) may be given in terms of a continuous distribution of crack aspect ratio and orientation as

$$\epsilon c^1_{ipjq} = -\frac{\epsilon_0}{\mu} c^0_{krip} c^0_{usjq} \tilde{T}_{krus}, \tag{16}$$

where

$$\begin{aligned}\tilde{T}_{krus} = \frac{8}{3}(1-\nu)\int_\Lambda dn^{\mathrm{c}} \Bigg\{ & n_r n_s \left[\frac{2}{2-\nu}(l_{1k}l_{1u} + l_{2k}l_{2u}) \right.\\ & \left. \times \frac{\alpha}{\alpha - i\omega\tau K_1} + n_k n_u \frac{1-i\omega\tau}{1-i\omega\tau\gamma}\right] \\ & - \alpha(\gamma-1)\frac{n_k n_r}{1-i\omega\tau\gamma}\left(\int_\Lambda dn^{\mathrm{c}} \frac{n_u n_s}{1-i\omega\tau\gamma}\right) \\ & \times \left(\int_\Lambda dn^{\mathrm{c}} \frac{\alpha\gamma}{1-i\omega\tau\gamma} + i\omega\tau K_2\right)^{-1}\Bigg\},\end{aligned} \tag{17}$$

where

$$\gamma \equiv \gamma(\alpha) = 1 + \frac{2\kappa_{\mathrm{f}}(1-\nu)}{\pi\mu\alpha}. \tag{18}$$

Here κ is the bulk modulus of the matrix, ω is the frequency and $\{l_{ij}\}$ is the rotation matrix from the background axes for a crack with normal in direction $\mathbf{n}$, to axes with normal in the x_3-direction. We write

$$dn^{\mathrm{c}} = n^{\mathrm{c}}(\alpha; \boldsymbol{\sigma}, p_{\mathrm{f}}, \theta, \phi)\, d\alpha\, d\Omega \tag{19}$$

for the probability density of cracks in the elemental volume $d\alpha\, d\Omega$, such that

$$\int_{\Lambda_0} n^{\mathrm{c}}(\alpha; \mathbf{0}, 0, \theta, \phi)\, d\alpha\, d\Omega = 1. \tag{20}$$

$d\Omega$ is the solid angle $\sin\theta\, d\theta\, d\phi$ and integration is over the volume $\Lambda \subseteq \Lambda_0 \equiv \mathbb{R}_+ \times \Omega$, where Ω is the region $0 \le \theta \le \pi/2$, $0 \le \phi \le 2\pi$ and the angular dependence is defined such that $\theta = 0$ corresponds to the x_3-direction. Λ may differ from Λ_0 by, for example, excluding a region of Λ in which no cracks remain on application of a sufficient compressive stress. ϵ_0 is the crack density in the absence of an applied stress or fluid pressure and the non-dimensional constants K_1 are K_2 are defined as

$$K_1 = \frac{4(1-\nu)\eta_{\mathrm{f}}}{(2-\nu)\pi\mu\tau} \tag{21}$$

and

$$K_2 = \frac{3\kappa_{\mathrm{f}}\hat{k}_p K^r_{pq}\hat{k}_q}{4\pi\epsilon_0 v^2\tau\eta_{\mathrm{f}}}, \tag{22}$$

where $\hat{\mathbf{k}}$ is the normalized wavenumber—the wavenumber divided by its magnitude—and v is a zeroth-order approximation to the wave speed of the incident wave. K_1 and K_2 are related to the constants P^m and P^k used in Tod (2001).

A term $(-\kappa_{\mathrm{f}}/\kappa)$ is neglected from the expression for γ (eq. 18), which had been retained by Tod (2001) though previously ignored by Hudson *et al.* (1996). While Thomsen (1995) retains this term, it was originally neglected in Hudson (1981). Retention of the term here breaks the necessary symmetry $\tilde{T}_{krus} = \tilde{T}_{uskr}$ when the crack aspect ratio distribution is orientation-dependent. This lack of symmetry was not therefore evident in Tod (2001) as only independent distributions were considered. It is anticipated that this lack of symmetry is a result of the inconsistency between Tod (2001) and Hudson (1981). Furthermore, it was found in Tod (2001) that it was necessary to disregard this term in order for the effective elastic constants to be consistent with Brown & Korringa (1975) in the low-frequency limit.

Exploiting the symmetries of eq. (16), we may replace $\tilde{T}_{krus}$ in eq. (16) with $\tilde{S}_{krus}$, where

$$4\tilde{S}_{krus} \equiv \tilde{T}_{krus} + \tilde{T}_{krsu} + \tilde{T}_{rkus} + \tilde{T}_{rksu}, \tag{23}$$

such that

$$\epsilon c^1_{ipjq} = -\frac{\epsilon_0}{\mu} c^0_{krip} c^0_{usjq} \tilde{S}_{krus} \tag{24}$$

and

$$\epsilon s^1_{ipjq} = \frac{\epsilon_0}{\mu}\tilde{S}_{ipjq}, \tag{25}$$

where the elastic compliances are of the form

$$\boldsymbol{s} = \boldsymbol{s}^0 + \epsilon\boldsymbol{s}^1 + \mathcal{O}(\epsilon^2) \tag{26}$$

and

$$s^0_{ipjq} = -\frac{\lambda}{2\mu(3\lambda+2\mu)}\delta_{ip}\delta_{jq} + \frac{1}{4\mu}(\delta_{ij}\delta_{pq} + \delta_{iq}\delta_{jp}). \tag{27}$$

An expression relating the first-order correction to the elastic compliances to the first-order correction to the elastic stiffnesses can be found in Tod (2001).

The total crack density ϵ is given by

$$\epsilon(\boldsymbol{\sigma}, p_{\mathrm{f}}) = \epsilon_0 \int_\Lambda dn^{\mathrm{c}}. \tag{28}$$

We make the simplifying assumption that in the absence of any applied stress or fluid pressure the distribution of cracks is independent of the crack normal orientation;

$$n^{\mathrm{c}}(\alpha; \mathbf{0}, 0, \theta, \phi) = n^{\mathrm{c}}_0(\alpha), \tag{29}$$

though by choosing otherwise, we may account for the effects of anisotropic paleostresses.

Using eq. (5) we may then write

$$n^{\rm c}(\alpha;\boldsymbol{\sigma},\, p_{\rm f},\theta,\phi) = \begin{cases} n_0^{\rm c}[\alpha - f(\boldsymbol{\sigma},\, p_{\rm f},\theta,\phi)] & \alpha \geq \max\{f(\boldsymbol{\sigma},\, p_{\rm f},\theta,\phi),0\} \\ 0 & \text{otherwise,} \end{cases} \tag{30}$$

where

$$f(\boldsymbol{\sigma},\, p_{\rm f},\theta,\phi) = \frac{2(1-\nu)}{\pi\mu}(\sigma_{ij}n_in_j + p_{\rm f}). \tag{31}$$

Restricting attention to the three compressive stresses (eqs 10–12), we have that the crack distribution is transversely isotropic about the x_3-axis for uniaxial or biaxial compression and isotropic for hydrostatic compression. In all three cases, the function f (eq. 31) is independent of the polar angle ϕ.

As an approximation to the initial crack aspect ratio distribution $n_0^{\rm c}(\alpha)$, we use an exponential distribution, Exp$(1/\alpha_0)$ (e.g. Ross 1989);

$$n_0^{\rm c}(\alpha) = \frac{1}{2\pi\alpha_0}{\rm e}^{-\alpha/\alpha_0} \quad \text{for} \quad 0 \leq \alpha, \tag{32}$$

where now α_0 denotes the average aspect ratio in the absence of stress and fluid pressure.

The resulting crack density is given by

$$\epsilon(\sigma,\, p_{\rm f}) = \epsilon_0 \int_0^{\pi/2} {\rm e}^{-g(\sigma,\, p_{\rm f},\theta)}\sin\theta\, d\theta, \tag{33}$$

where

$$g(\sigma,\, p_{\rm f},\theta) = \max\{-f(\sigma,\, p_{\rm f},\theta)/\alpha_0,\, 0\}. \tag{34}$$

Taking $v_P = 4.2\times10^3$ m s^{-1}, $v_S = 2.7\times10^3$ m s^{-1}, $\rho = 2.49\times10^3$ kg m^{-3}, corresponding to the sandstone of model 1 in Sayers & Rickett (1997), $\epsilon_0 = 0.3$ and $\alpha_0 = 5.0\times10^{-4}$, then under hydrostatic stress the crack density is given by

$$\epsilon(\sigma,\, p_{\rm f}) = \epsilon_0{\rm e}^{-c_r\, p_{\rm d}} \quad \text{for} \quad p_{\rm d} \geq 0, \tag{35}$$

where we define

$$c_r = \frac{2(1-\nu)}{\pi\mu\alpha_0} \tag{36}$$

and for the choice of parameters above, $c_r = 6.0\times10^{-8}$ Pa^{-1}, in good agreement with Zhang & Bentley (2000) and Chapman (2001).

The corresponding expressions for biaxial and uniaxial compression are given by

$$\epsilon(\sigma,\, p_{\rm f}) = \epsilon_0\left[1 - \sqrt{\frac{p_{\rm d}}{\sigma}} - \frac{i}{2}{\rm e}^{-c_r\, p_{\rm d}}\sqrt{\frac{\pi}{c_r\sigma}}\,{\rm erf}(i\sqrt{c_r\, p_{\rm d}})\right] \quad \text{for} \quad p_{\rm d} \geq 0 \tag{37}$$

and

$$\epsilon(\sigma,\, p_{\rm f}) = \epsilon_0\left\{\sqrt{\frac{p_{\rm f}}{\sigma}} + \frac{1}{2}{\rm e}^{c_r\, p_{\rm f}}\sqrt{\frac{\pi}{c_r\sigma}}[{\rm erf}(\sqrt{c_r\sigma}) - {\rm erf}(\sqrt{c_r\, p_{\rm f}})]\right\} \quad \text{for} \quad p_{\rm d} \geq 0, \tag{38}$$

respectively, where erf(x) is the error function (e.g. Gradshteyn & Ryzhik 1980). In all three cases $\epsilon = \epsilon_0$ for $p_{\rm d} \leq 0$. We note that $i\,{\rm erf}(ix)$ (eq. 37) is real.

We may simplify eq. (17) considerably in the zero-frequency limit when the initial crack distribution is given by eq. (32). Representing the scaled compliance tensor $\tilde{S}_{krus}$ in terms of the conventional condensed, two-subscript, 6×6 matrix notation, $\tilde{S}_{ij}$, say, pairs of indices are represented as a single index: $kr \to i$, $us \to j$, such that $11 \to 1$, $22 \to 2$, $33 \to 3$, $23 \to 4$, $13 \to 5$ and $12 \to 6$. Furthermore, a multiplicative factor of 2 is introduced if one of the indices i or j is greater than 3 and a factor of 4 if both of them are. We find that when $p_{\rm d} \leq 0$,

$$\begin{aligned}\tilde{S}_{12} &= \frac{8}{3}(1-\nu)\left\{-\frac{1}{15}\frac{2}{2-\nu} + \frac{1}{15} - \frac{2\kappa_{\rm f}(1-\nu)}{9\pi\mu}\right. \\ &\quad \left.\times\left[\alpha_0\gamma_0 - \frac{2(1-\nu)}{\pi\mu}\left(\frac{n}{3}\sigma - p_{\rm f}\right)\right]^{-1}\right\} \\ &= \tilde{S}_{13} = \tilde{S}_{23},\end{aligned} \tag{39}$$

$$\begin{aligned}\tilde{S}_{66} &= \frac{32}{3}(1-\nu)\left(\frac{1}{10}\frac{2}{2-\nu} + \frac{1}{15}\right) \\ &= \tilde{S}_{44} = \tilde{S}_{55}\end{aligned} \tag{40}$$

and

$$\begin{aligned}\tilde{S}_{11} &= \tilde{S}_{12} + \frac{1}{2}\tilde{S}_{66} \\ &= \tilde{S}_{22} = \tilde{S}_{33},\end{aligned} \tag{41}$$

where $n = 1$, 2 and 3 for uniaxial, biaxial and hydrostatic compression, respectively, and $\gamma_0 \equiv \gamma\,(0)$ (eq. 18). Thus, $\boldsymbol{c}$ (eq. 3) is isotropic and we may write the perturbations to the Lamé constants as

$$\lambda \to \lambda - \epsilon_0\left[\left(9\frac{\lambda^2}{\mu} + 12\lambda + 4\mu\right)\tilde{S}_{12} + \left(\frac{3}{2}\frac{\lambda^2}{\mu} + 2\lambda\right)\tilde{S}_{66}\right] \tag{42}$$

and

$$\mu \to \mu - \epsilon_0\mu\tilde{S}_{66}. \tag{43}$$

For $p_{\rm d} \geq 0$, under hydrostatic compression, $\boldsymbol{S}$ retains the same symmetries as the above, but with

$$\begin{aligned}\tilde{S}_{12} &= \frac{8}{3}(1-\nu){\rm e}^{-c_r\, p_{\rm d}}\left\{-\frac{1}{15}\frac{2}{2-\nu} + \frac{1}{15} - \frac{2\kappa_{\rm f}(1-\nu)}{9\pi\mu}\right. \\ &\quad \left.\times\left[\alpha_0\gamma_0 - \frac{2(1-\nu)}{\pi\mu}p_{\rm d}\right]^{-1}\right\}\end{aligned} \tag{44}$$

and

$$\tilde{S}_{66} = \frac{32}{3}\,(1-\nu)\,{\rm e}^{-c_r\, p_{\rm d}}\left(\frac{1}{10}\frac{2}{2-\nu} + \frac{1}{15}\right). \tag{45}$$

Under either biaxial or uniaxial compression $\tilde{\boldsymbol{S}}$ loses some of its symmetries and the resulting expression for $\boldsymbol{c}$ has five independent components.

5 RESULTS

We assume that $\{K^r_{pq}\} = K^r\delta_{pq}$ and take $K^r = 10^3$ mD ($\simeq10^{-12}$ m^2), $\kappa_{\rm f} = 2.25\times10^9$ Pa and $\eta_{\rm f} = 10^{-3}$ Pa s. Taking $\tau = 10^{-5}$ s, and assuming that the incident wave is of compression-wave type, with frequency 50 rad s^{-1}, the non-dimensional constants become $K_1 = 3.2\times10^{-9}$, $K_2 = 1.0\times10^{-2}$ and $\omega\tau = 5.0\times10^{-4}$.

When the differential pressure $p_{\rm d}$ (eq. 13) is negative, that is $\sigma/p_{\rm f} < 1$, there is no crack closure, thus no change in crack density. However, the change in crack aspect ratio is orientation-dependent, so that the effective medium exhibits minor anisotropy.

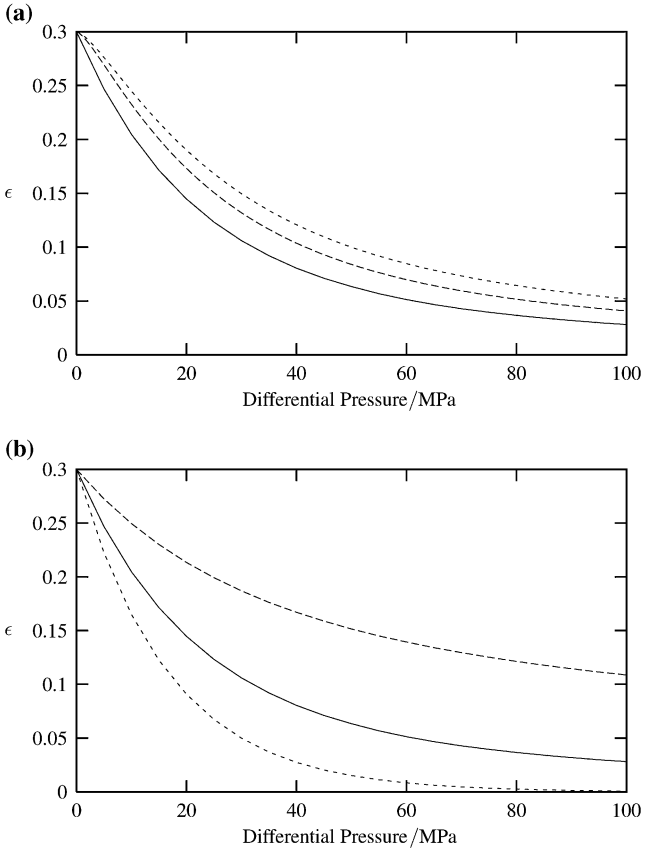

Figure 1. (a) Crack density ϵ as a function of differential pressure at 0 MPa (solid line), 10 MPa (long dashes) and 20 MPa (short dashes) fluid pressure, under biaxial compression. (b) Crack density as a function of differential pressure for fluid pressure 0 MPa under biaxial (solid line), uniaxial (long dashes) and hydrostatic (short dashes) compression.

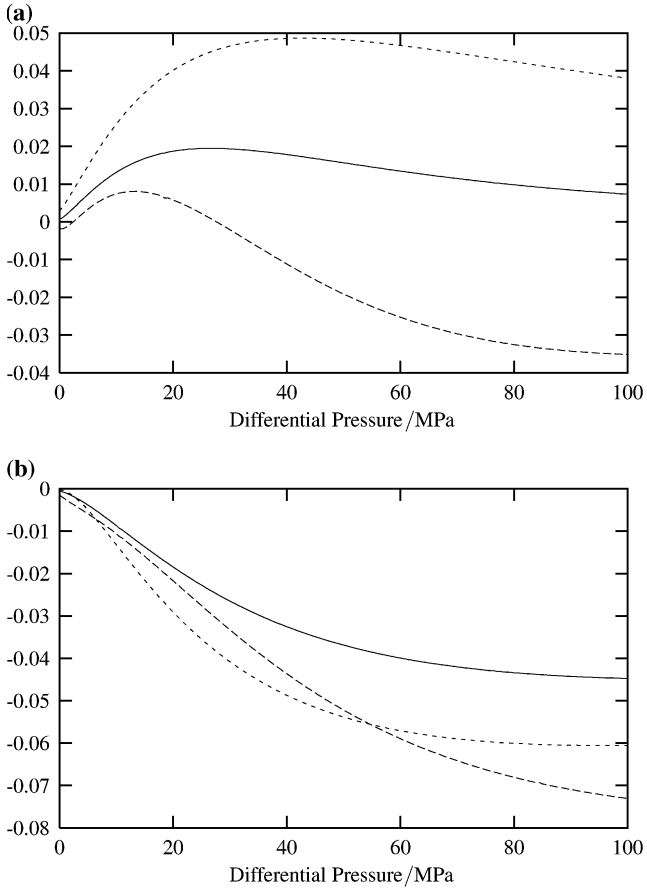

Figure 2. (a) Thomsen's parameters ϵ_T (solid line), δ_T (long dashes) and γ_T (short dashes) as a function of differential pressure at a fluid pressure of 20 MPa, under biaxial compression. (b) As in (a), except under uniaxial compression.

Once $\sigma/p_f > 1$, preferentially oriented crack closure occurs and the crack density decreases with increasing compressive biaxial stress (Fig. 1a). At large stresses only those cracks with normals lying in, or close to, the x_3-direction remain open. The presence of a non-zero pressure within the fluid medium increases the crack density at any given value of the compressive stress, as it hinders the process of crack closure (Fig. 1a). Crack density decreases faster, as a function of differential pressure, for hydrostatic compression (eq. 12) than for biaxial compression (eq. 11), (Fig. 1b), which in turn decreases faster than for uniaxial compression (eq. 10).

The anisotropy of the effective medium is measured using Thomsen's parameters; ϵ_T, δ_T and γ_T (eqs A1–A3) (Thomsen 1986). As can be seen (Figs 2a and b) all three of the parameters reach a maximal (absolute) value under biaxial or uniaxial compression before decaying towards zero at large differential pressure as the properties of the cracked aggregate approach those of the uncracked matrix. We notice that δ_T, a measure of the SH-wave anisotropy, reaches far larger values than ϵ_T, a measure of the P-wave anisotropy, and so is more likely to be detected. For uniaxial compression (Fig. 2b), peak values of the anisotropy parameters are reached at larger values of the differential pressure than for biaxial compression (Fig. 2a). This is largely as a result of the larger crack density at comparative differential pressures for uniaxial compression as opposed to biaxial compression.

For waves propagating in a direction parallel to the symmetry axis, there is no shear wave splitting, just two wave speeds. Both of these wave speeds are seen to increase with differential pressure (Figs 3a–c), approaching the matrix wave speeds at large pressures. For a biaxial (Fig. 3a) or hydrostatic (Fig. 3c) compression the shear wave speed shows a significantly greater proportional change with pressure than the compressional wave speed does, indicating that shear waves are more sensitive to pressure changes than compressional ones. However, for a uniaxial compression (Fig. 3b) this difference is only very slight. Comparing the wave speeds at different fluid pressures for biaxial and uniaxial compression (Figs 3a and b), we notice that a non-zero fluid pressure decreases the rate at which the wave speeds increase towards the uncracked isotropic values. At increasingly negative differential pressure both compressional and shear wave speeds continue to decrease, though only marginally (not shown). Under hydrostatic compression the wave speeds, as a function of differential pressure, are independent of fluid pressure. This is as expected, since, from eqs (12) and (31), the function f is independent of the angular variables. Indeed, f is linear in p_d (eq. 13).

At an angle of incidence normal to the symmetry axis, we see shear wave splitting (Figs 4a and b). For biaxial compression (Fig. 4a) the wave speed of the SH wave increases faster than that of the SV wave. Also, the wave speed of the P wave decreases faster at normal incidence than it does at parallel incidence (*cf.* Fig. 3a). Both of the trends are reversed for uniaxial compression (Fig. 4b and 3b). The level of shear wave splitting, as a function of differential pressure, at normal incidence corresponds to the change

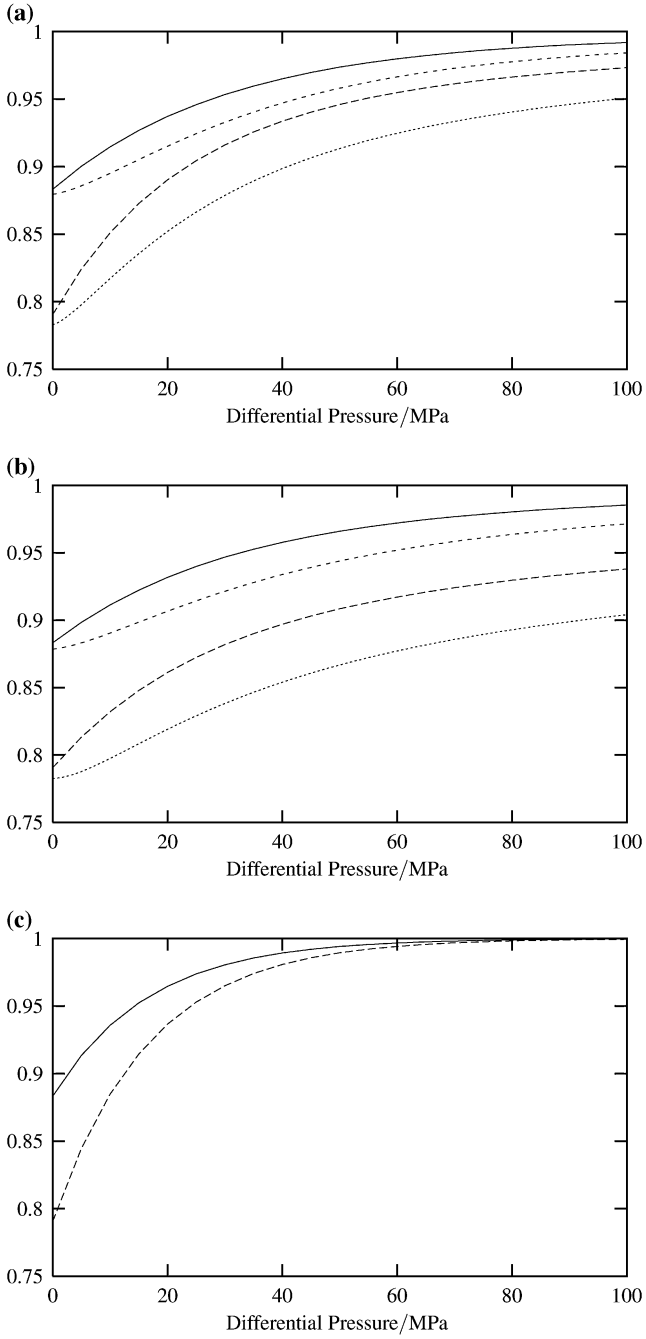

Figure 3. (a) Compressional (solid line and medium dashes) and shear wave speeds (long dashes and short dashes) normalized by their values in the isotropic uncracked matrix, as a function of differential pressure, at fluid pressures of 0 and 20 MPa, respectively, at incidence parallel to the direction of symmetry, under biaxial compression. (b) As in (a), except under uniaxial compression. (c) As in (a), except under hydrostatic compression, but only at a fluid pressure of 0 MPa; compressional wave speed (solid line) and shear wave speed (dashes).

in Thomsen's parameter γ_T with differential pressure—indeed γ_T is equal to the difference between the two shear wave speeds at normal incidence, to first order in the crack density ϵ.

With no shear wave splitting at parallel incidence, we only have two attenuation coefficients (Figs 5a–c), that peak in value at differential pressures corresponding to the points at which the corresponding wave speeds are changing most rapidly (Figs 3a and b).

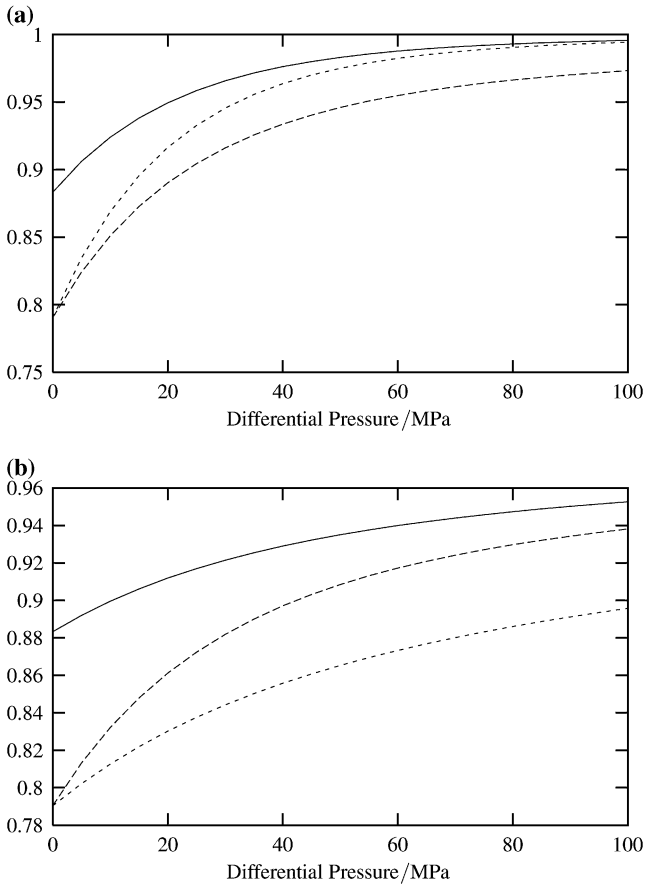

Figure 4. (a) Normalized compressional (solid line) and vertically and horizontally polarized shear wave speeds (long dashes, short dashes) as a function of differential pressure, at a fluid pressure of 0 MPa, at incidence normal to the direction of symmetry, under biaxial compression. (b) As in (a), except under uniaxial compression.

The *S*-wave attenuation is everywhere greater than the *P*-wave attenuation. Fluid pressure is seen to reduce the attenuation at low differential pressures, while increasing it at higher differential pressures. As with the wave speeds, both the *P*- and *S*-wave attenuation coefficients continue to decrease for increasingly negative differential pressure (not shown). A similar behaviour is seen with hydrostatic compression (Fig. 5c), where the attenuation coefficients as functions of differential pressure are independent of fluid pressure, as were the wave speeds under hydrostatic compression. This attenuation is a direct result of the presence of a local fluid flow.

6 CONCLUSIONS

The model proposed by Hudson *et al.* (1996) for the transfer of fluid between connected cracks via non-compliant pores and extended by Tod (2001) to allow for a continuous distribution of values of both crack orientation and aspect ratio has been further extended to allow these distributions to depend upon each other via the applied stress and fluid pressure, using the results of Hudson (2000).

The pressure effects are included via a mechanism that allows for the collapse and closure of the cracks present in an unstressed state, and does not allow for the possible growth of existing cracks, the deformation of pores into cracks, or the formation of new cracks. This leads to a description that is purely elastic under loading and unloading, rather than one that exhibits hysteresis. Furthermore,

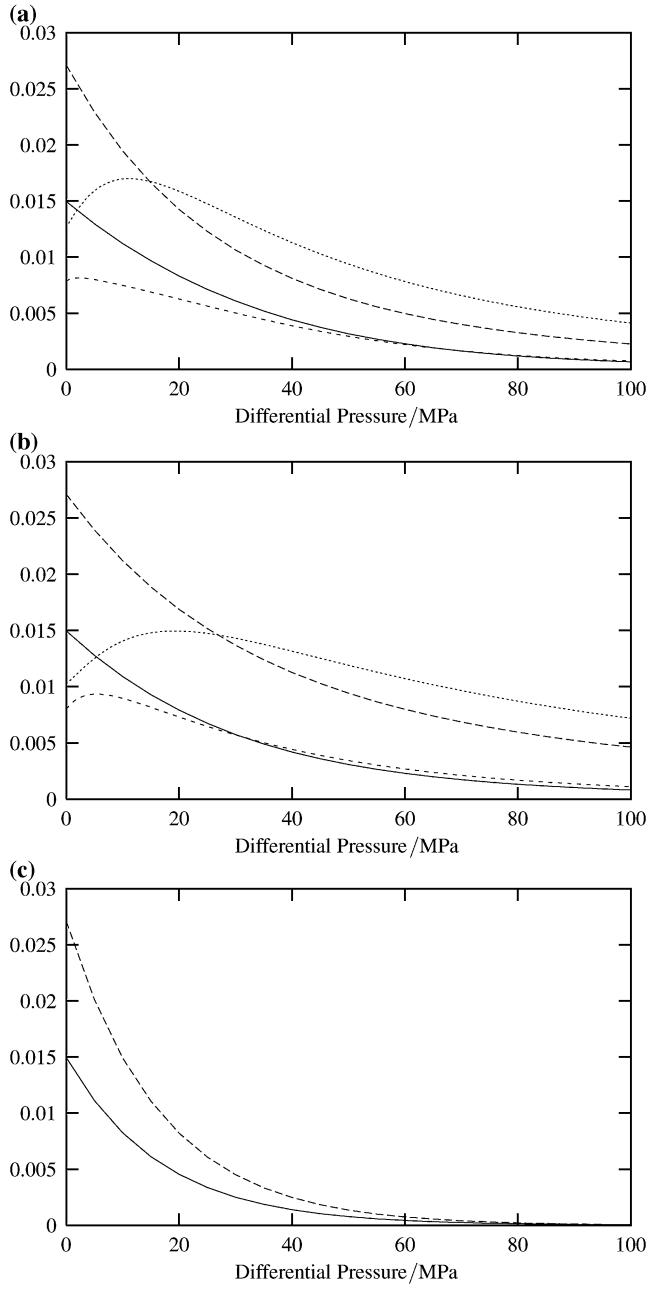

Figure 5. (a) Compressional (solid line, medium dashes) and shear attenuation coefficients (long dashes, short dashes) as a function of differential pressure, at fluid pressures of 0 and 20 MPa, respectively, at incidence parallel to the direction of symmetry, under biaxial compression. (b) As in (a), except under uniaxial compression. (c) As in (a), except under hydrostatic compression, and only at a fluid pressure of 0 MPa; compressional (solid line) and shear (dashes) attenuation coefficients.

stress history is not accounted for in the model, by assuming that in the unstressed state the crack distribution is isotropic. We may, however, remedy this by including an initial crack distribution that is anisotropic. This would increase the magnitude of the anisotropy parameters.

While the effect of an increase in the differential pressure will increase the polarization of the distribution of remaining cracks, which will serve to increase the anisotropy, the total crack density will decrease, thus decreasing the anisotropy. These two competing processes explain the rise in the anisotropy parameters with differential pressure (Figs 2a and b) to a maximum absolute value, before a decay towards zero as the differential pressure increases yet further, as the properties of the effective material approach those of the isotropic matrix—in this large pressure limit, all of the original cracks are effectively closed, so that the material resembles the uncracked isotropic matrix.

The predicted increase in wave speed with differential pressure agrees with other theoretical models (Nur 1971; Toksöz *et al.* 1976; Cheng & Toksöz 1979; Carlson & Gangi 1985; Pecorari 1997; Sun & Goldberg 1997) and experimental results (Winkler 1985; Freund 1992; Hornby 1994). That the *S*-wave attenuation is greater than that for the *P* waves agrees with other low-porosity theories, though the two are reversed at higher porosities (Chapman 2001).

This model of an effective medium theory may be combined with a model of a fault (e.g. Tod & Hudson 2001) or used in a full-waveform or a ray-tracing modelling package to produce synthetic seismograms, which may be compared with surface seismics or VSP data.

ACKNOWLEDGMENTS

The author would like to thank John A. Hudson at DAMTP, University of Cambridge and Enru Liu at the British Geological Survey for support and encouragement. The work was sponsored by the Natural Environment Research Council through project GST022305, as part of the thematic programme *Understanding the micro-to-macro behaviour of rock fluid systems* ($\mu 2M$) and is published with the approval of the Director of the British Geological Survey.

REFERENCES

Bai, T., Pollard, D.D. & Gross, M.R., 2000. Mechanical prediction of fracture aperture in layered rocks, *J. geophys. Res.,* **105,** 707–721.

Brown, R.J.S. & Korringa, J., 1975. On the dependence of the elastic properties of a porous rock on the compressibility of the pore fluid, *Geophysics,* **40,** 608–616.

Brown, S.R. & Scholz, C.H., 1986. Closure of rock joints, *J. geophys. Res.,* **91,** 4939–4948.

Carlson, R.L. & Gangi, A.F., 1985. Effect of cracks on the pressure dependence of *P* wave velocities in crystalline rocks, *J. geophys. Res.,* **90,** 8675–8684.

Chapman, M., 2001. Modelling the wide-band laboratory response of rock samples to fluid and pressure changes, *PhD thesis,* University of Edinburgh.

Cheng, C.H. & Toksöz, M.N., 1979. Inversion of seismic velocities for the pore aspect ratio spectrum of a rock, *J. geophys. Res.,* **84,** 7533–7543.

Fredrich, J.T. & Wong, T.-F., 1986. Micromechanics of thermally induced cracking in three crustal rocks, *J. geophys. Res.,* **91,** 12 743–12 764.

Freund, D., 1992. Ultrasonic compressional and shear velocities in dry clastic rocks as a function of porosity, clay content, and confining pressure, *Geophys. J. Int.,* **108,** 125–135.

Gangi, A.F. & Carlson, R.L., 1996. An asperity-deformation model for effective pressure, *Tectonophysics,* **256,** 241–251.

Gibson, R.L. & Toksöz, M.N., 1990. Permeability estimation from velocity anisotropy in fractured rock, *J. geophys. Res.,* **95,** 15 643–15 655.

Gradshteyn, I.S. & Ryzhik, I.M., 1980. *Tables of Integrals, Series, and Products,* 4th edn, Academic Press, New York.

Horii, H. & Nemat-Nasser, S., 1983. Overall moduli of solids with microcracks: load-induced anisotropy, *J. Mech. Phys. Solids,* **31,** 155–171.

Hornby, B.E., 1994. The elastic properties of shales, *PhD thesis,* University of Cambridge.

Hudson, J.A., 1980. Overall properties of a cracked solid, *Math. Proc. Camb. Phil. Soc.,* **88,** 371–384.

Hudson, J.A., 1981. Wave speeds and attenuation of elastic waves in material containing cracks, *Geophys. J. R. astr. Soc.,* **64,** 133–150.
Hudson, J.A., 2000. The effect of fluid pressure on wavespeeds in a cracked solid, *Geophys. J. Int.,* **143,** 302–310.
Hudson, J.A., Liu, E. & Crampin, S., 1996. The mechanical properties of materials with interconnected cracks and pores, *Geophys. J. Int.,* **124,** 105–112.
Kuster, G.T. & Toksöz, M.N., 1974. Velocity and attenuation of seismic waves in two-phase media: part 1. Theoretical formulations, *Geophysics,* **39,** 587–606.
Li, C. & Nordlund, E., 1993. Deformation of brittle rocks under compression—with particular reference to microcracks, *Mech. Mater.,* **15,** 223–239.
Menéndez, B., David, C. & Darot, M., 1999. A study of the crack network in thermally and mechanically cracked granite samples using confocal scanning laser microscopy, *Phys. Chem. Earth* A, **24,** 627–632.
Montoto, M., Martínez-Nistal, A., Rodríguez-Rey, A., Fernández-Merayo, N. & Soriano, P., 1995. Microfractography of granite rocks under confocal scanning laser microscopy, *J. Microscopy,* **177,** 138–149.
Nur, A., 1971. Effects of stress on velocity anisotropy in rocks with cracks, *J. geophys. Res.,* **76,** 2022–2034.
Pecorari, C., 1997. Acoustoelasticity in cracked solids, *Geophys. J. Int.,* **129,** 169–175.
Ross, S.M., 1989. *Probability Models,* 4th edn, Academic, San Diego, CA.
Sayers, C.M., 1988a. Inversion of ultrasonic wave velocity measurements to obtain the microcrack orientation distribution function in rocks, *Ultrasonics,* **26,** 73–77.
Sayers, C.M., 1988b. Stress-induced ultrasonic wave velocity anisotropy in fractured rock, *Ultrasonics,* **26,** 311–317.
Sayers, C.M. & Rickett, J.E., 1997. Azimuthal variation in AVO response for fractured gas sands, *Geophys. Prospect.,* **45,** 165–182.
Sun, Y.F. & Goldberg, D., 1997. Estimation of aspect-ratio changes with pressure from seismic velocities, in *Developments in Petrophysics,* Vol. 122, pp. 131–139, eds Lovell, M.A. & Harvey, P.K., Geological Society Special Publication, The Geological Society, London.
Thomsen, L., 1986. Weak elastic anisotropy, *Geophysics,* **51,** 1954–1966.
Thomsen, L., 1995. Elastic anisotropy due to aligned cracks in porous rock, *Geophys. Prospect.,* **43,** 805–829.
Tod, S.R., 2001. The effects on seismic waves of interconnected nearly aligned cracks, *Geophys. J. Int.,* **146,** 249–263.
Tod, S.R. & Hudson, J.A., 2001. Continuity conditions for a fault consisting of obliquely aligned cracks, *Geophys. J. Int.,* **144,** 679–684.
Toksöz, M.N., Cheng, C.H. & Timur, A., 1976. Velocities of seismic waves in porous rocks, *Geophysics,* **41,** 621–645.
Walsh, J.B., 1965a. The effect of cracks on the compressibility of rock, *J. geophys. Res.,* **70,** 381–389.
Walsh, J.B., 1965b. The effect of cracks on the uniaxial elastic compression of rocks, *J. geophys. Res.,* **70,** 399–411.
Winkler, K.W., 1985. Dispersion analysis of velocity and attenuation in berea sandstone, *J. geophys. Res.,* **90,** 6793–6800.
Wulff, A.-M., Hashida, T., Watanabe, K. & Takahashi, H., 1999. Attenuation behaviour of tuffaceous sandstone and granite during microfracturing, *Geophys. J. Int.,* **139,** 395–409.
Zatsepin, S.V. & Crampin, S., 1997. Modelling the compliance of crustal rock—1. Response of shear-wave splitting to differential pressure, *Geophys. J. Int.,* **129,** 477–494.
Zhang, J.J. & Bentley, L.R., 2000. Change of elastic moduli of dry sandstone with effective pressure, in *70th Ann. Int. Mtg SEG, Exp. Abs.,* pp. 1826–1829.

APPENDIX A: THOMSEN'S PARAMETERS, WAVE SPEEDS AND ATTENUATION COEFFICIENTS

In the conventional condensed, two-subscript, 6×6 matrix notation, pairs of indices are represented as a single index: $ij \to p$, $kl \to q$, such that $11 \to 1$, $22 \to 2$, $33 \to 3$, $23 \to 4$, $13 \to 5$ and $12 \to 6$. We thus use the representation C_{pq}, rather than c_{ijkl}.

We make use of the anisotropy parameters defined by Thomsen (1986) for transversely isotropic material with symmetry axis in the x_3-direction:

$$\epsilon_{\mathrm{T}} \equiv \frac{C_{11} - C_{33}}{2C_{33}}, \tag{A1}$$

$$\delta_{\mathrm{T}} \equiv \frac{(C_{13} + C_{44})^2 - (C_{33} - C_{44})^2}{2C_{33}(C_{33} - C_{44})}, \tag{A2}$$

$$\gamma_{\mathrm{T}} \equiv \frac{C_{66} - C_{44}}{2C_{44}}, \tag{A3}$$

where the real part is assumed when the stiffnesses are complex.

For an incident wave, whose direction of propagation is at an angle θ to the symmetry axis, the perturbation to the wave speeds and attenuation coefficients, to first order in crack density ϵ, are given by Tod (2001) as

$$\frac{v_{qP}}{v_P} = 1 + \frac{\epsilon}{2(\lambda + 2\mu)} \mathrm{Re}\left(\sin^4\theta C^1_{11} + \cos^4\theta C^1_{33} + \frac{1}{2}\sin^2 2\theta C^1_{13} + \sin^2 2\theta C^1_{44} \right), \tag{A4}$$

$$\frac{v_{qSV}}{v_S} = 1 + \frac{\epsilon}{2\mu} \mathrm{Re}\left(\frac{1}{4}\sin^2 2\theta \left(C^1_{11} + C^1_{33} - 2C^1_{13} \right) + \cos^2 2\theta C^1_{44} \right), \tag{A5}$$

$$\frac{v_{qSH}}{v_S} = 1 + \frac{\epsilon}{2\mu} \mathrm{Re}\left(\cos^2\theta C^1_{44} + \sin^2\theta C^1_{66} \right) \tag{A6}$$

and

$$Q^{-1}_{qP} = \frac{\epsilon}{\lambda + 2\mu} \left| \mathrm{Im}\left(\sin^4\theta C^1_{11} + \cos^4\theta C^1_{33} + \frac{1}{2}\sin^2 2\theta C^1_{13} + \sin^2 2\theta C^1_{44} \right) \right|, \tag{A7}$$

$$Q^{-1}_{qSV} = \frac{\epsilon}{\mu} \left| \mathrm{Im}\left(\frac{1}{4}\sin^2 2\theta \left(C^1_{11} + C^1_{33} - 2C^1_{13} \right) + \cos^2 2\theta C^1_{44} \right) \right|, \tag{A8}$$

$$Q^{-1}_{qSH} = \frac{\epsilon}{\mu} \left| \mathrm{Im}\left(\cos^2\theta C^1_{44} + \sin^2\theta C^1_{66} \right) \right|. \tag{A9}$$